Journal of Membrane Science 603 (2020) 117921

Contents lists available at ScienceDirect

Journal of Membrane Science

journal homepage: http://www.elsevier.com/locate/memsci

Energy barriers to anion transport in polyelectrolyte multilayer nanofiltration membranes: Role of intra-pore diffusion

Sigyn B. Sigurdardottir [a,b], Ryan M. DuChanois [a], Razi Epsztein [a,c,**], Manuel Pinelo [b], Menachem Elimelech [a,*]

[a] Department of Chemical and Environmental Engineering, Yale University, New Haven, CT, 06520-8286, USA
[b] Department of Chemical and Biochemical Engineering, Technical University of Denmark, DTU, Søltofts Plads, Building 229, 2800, Kgs, Lyngby, Denmark
[c] Faculty of Civil and Environmental Engineering, Technion – Israel Institute of Technology, Haifa 32000, Israel

ARTICLE INFO

Keywords:
Nanofiltration membrane
Energy barrier
Layer-by-layer assembly
Membrane thickness
Ion transport

ABSTRACT

We investigated the relative contributions of intra-pore diffusion (via membrane thickness) and partitioning into nanofiltration (NF) membrane pores (via membrane pore size and ion hydration energy) to the apparent energy barriers for ion transport in NF membranes. Using polyelectrolyte layer-by-layer assembly, we independently altered NF membrane thickness as well as membrane pore size and then determined the apparent energy barriers to bromide and fluoride transport through the fabricated membranes. Membrane thickness and pore size were estimated using an AFM scratch technique and the hydrodynamic pore transport model, respectively. By increasing the number of polyelectrolyte bilayers from four to ten, the polyelectrolyte film thickness increased from 28 to 77 nm, while the apparent energy barriers to bromide transport through the membranes with four, seven, and ten bilayers were negligibly affected (4.4, 3.4, and 3.9 kcal mol^{-1}, respectively, at 1.7 bar). Instead, we found that solute flux and the apparent energy barriers to ion transport were significantly affected by both membrane pore size and ion hydration energy. Overall, our results support the traditional energy barrier-based models for ion transport in membranes and the recently proposed notion that ion dehydration at the solution-membrane interface is the rate-limiting step during transport through NF membranes.

1. Introduction

Nanofiltration (NF) is a pressure-driven membrane separation process in which a semi-permeable membrane acts as a selective barrier that separates salts and low molecular-weight solutes from a solution [1–3]. The separation properties of NF membranes lie between those of reverse osmosis (RO) and ultrafiltration (UF) membranes, and thus the solute transport mechanism in NF membranes is based on both diffusion and convection, as well as electromigration [4,5]. The most recognized solute rejection mechanisms of NF membranes are Donnan (charge) and steric (size) exclusion [6–8], which can be exploited for the removal of target solutes, product concentration, and solvent recovery from a feed stream [9–11]. Applications of NF (e.g., in the textile, food, pharmaceutical, and biorefinery industries) focus mainly on water softening and wastewater treatment [12–20].

As solute rejection in NF is mainly controlled by the size and charge of the membrane pores and the species passing through the pores [4], it follows that selectivity for species of similar size and charge is often limited [7,21–24]. Nevertheless, certain selectivity trends have been observed during the separation of ions of similar hydrated size and charge [22,25], which have mainly been ascribed to the respective hydration energies of the ions [22,26]. A higher hydration energy implies a higher energetic cost of ion dehydration, while the need for ion dehydration increases as the pore size decreases [22,25,27–33]. Numerous studies have demonstrated how higher hydration energy can enhance steric exclusion of an ion when the hydrated size of the ion is similar to the membrane pore size, since the water shells surrounding the ion are less easily removed or distorted during passage through the membrane pores [4,25,27,34–37]. Ion dehydration, as an ion-specific effect, can thus be considered an additional mechanism involved in ion selectivity.

Besides influencing ion rejection, ion hydration energy and dehydration are also reflected in the energy barrier to ion transport through NF membranes [37]. Energy barriers arise when a membrane imposes a hindrance to transport. The energy barriers amount to the energy

* Corresponding author.
** Corresponding author. Technion - Israel Institute of Technology, Israel.
E-mail addresses: raziepsztein@technion.ac.il (R. Epsztein), menachem.elimelech@yale.edu (M. Elimelech).

https://doi.org/10.1016/j.memsci.2020.117921
Received 23 October 2019; Received in revised form 23 December 2019; Accepted 2 February 2020
Available online 3 February 2020

required for solute transport to occur, which includes contributions from all transport mechanisms involved (convection, diffusion, and electrical mobility) [20,25]. Furthermore, the energy barriers due to diffusion depend on the respective rate constants for diffusion at the solution-membrane interface (solute partitioning into the membrane) and inside the membrane [38].

The transport of solutes through membranes with pore sizes similar to the size of the hydrated solute involves partitioning of the solutes into the membrane, followed by diffusion through the membrane [22,39]. The diffusion step can be described as solutes hopping between equilibrium positions, such as vacant sites [38,40] and sites of favorable chemical/electrostatic interactions [41–44]. Notably, the diffusion of dehydrated ions inside membrane pores is strongly influenced by local charge stabilization, as the point charge of the ions is exposed upon dehydration and thereby interacts more strongly with electrically charged sites of the pore walls. This transport has been described as jump diffusion and can lead to slower ion permeation through the membrane [44].

With the series of hindrances offered by the membrane pore entry and interior, the solutes can be considered to traverse multiple transition states during transport — i.e., momentary high-potential-energy and unstable configurations — much like those described by the transition-state theory for chemical reactions [40,45]. The energy barriers associated with the individual transition-states cannot be evaluated separately due to the limited number of measurable parameters involved in transport [38]. However, an apparent representative energy barrier to solute transport through membranes can be quantified experimentally using a single-barrier Arrhenius-type equation, which describes the solute flux (analogous to a chemical reaction rate constant) as a function of temperature [22,37,46].

Molecular dynamics simulations and ion transport experiments reveal that when the membrane pore size is similar to the hydrated size of the ion (such as in NF membranes), ion dehydration at the pore entry is the main contribution to the apparent energy barrier [22,25,46]. For instance, Corry et al. [28,29] investigated energy barriers to ion -transport in carbon nanotubes (CNTs) using molecular dynamics s-imulations, and showed that the energy barriers were controlled by the CNT diameter and the hydration energy of the ions, whereas the energy barriers were unaffected by the length of the CNTs. Unlike the frictionless transport in CNTs, polymeric NF membranes are tortuous, and the local chemical properties may vary throughout the length of the pores. Solutes experience various resistances during transport through such membranes, such as physical and chemical interactions with the pore walls [29], and they are assumed to overcome numerous transport-related energy barriers inside the membrane pores [29,38]. The contribution of these intra-pore energy barriers to the apparent energy barrier in NF membranes has yet to be shown experimentally. Notably, while energy barriers arise due to a series of local hindrances, the question whether the energy barrier for ion transport accumulates along the membrane thickness has not been answered. Hence, the contribution of the intra-pore energy barriers may be evaluated by investigating the effect of membrane thickness on the apparent energy barriers to transport in NF membranes.

NF membranes are generally composed of a thin, selective separation layer, and a thicker, porous support layer. The separation layer primarily controls transport through the membrane and is where energy barriers arise. The separation layer in commercial membranes is most commonly fabricated by interfacial polymerization, a technique where a polymeric film is synthesized at an aqueous-organic interface [5,14,18]. An alternative method for the fabrication of the separation layer is polyelectrolyte (PE) layer-by-layer (LbL) assembly. In this method, a polyelectrolyte multilayer (PEM) is assembled on top of the porous support by alternating deposition of oppositely charged PEs to form a film with separation performance in the range of NF membranes [6,8,47,48]. The LbL assembly method has gained attention for its simplicity and versatility [49].

The properties of PEM films can be controlled by numerous fabrication parameters. For instance, the pore size and layer thickness can be tuned by controlling the concentrations of PEs and background ionic strength of the deposition solutions [6], the film thickness can be increased by addition of layers [43,47,49–52], and the surface charge can be controlled by the terminating PE [7,16,43]. Moreover, the surface charge can be dramatically changed, or even reversed, by incorporating salt annealing in the fabrication procedure [41,53–55]. Given the highly controllable properties of PEM films, PE LbL assembly is a practical method for fabrication of tailor-made membranes for specific applications, such as investigating the effects of membrane thickness on the apparent energy barriers to ion transport through NF membranes.

In this work, we used PE LbL assembly to study energy barriers to ion transport in NF membranes of different thicknesses. By carefully controlling the LbL deposition conditions, we first fabricated PEM NF membranes of various thicknesses but similar pore size and surface charge. We then measured experimental energy barriers to ion transport through the membranes and found that (i) increased membrane thickness does not result in significantly higher energy barriers to ion permeation and (ii) the intra-pore diffusion creates a relatively low barrier. Conversely, we found that energy barriers are dependent on ion hydration energy as well as NF membranes pore size, corroborating previous experimental and molecular dynamics studies. Our work provides experimental evidence that energy barriers to ion transport in NF arise primarily due to ion dehydration effects at the water-membrane interface and can be used to guide the design of selective membrane materials.

2. Materials and methods

2.1. Materials and chemicals

Commercial polysulfone (PSf) ultrafiltration (UF) membranes (Sepro Membranes, Oceanside, CA, USA) with molecular weight cut-off of 20 kDa were used as the substrate for PE LbL self-assembly. Poly (diallyldimethylammoniumchloride) (PDADMAC; MW 150,000–200,000 g mol^{-1}; 20% wt. in water), poly(sodium 4-styrenesulfonate) (PSS; MW 70,000 g mol^{-1}), erythritol, glucose, xylose, sodium bromide (NaBr), and sodium fluoride (NaF) were purchased from Sigma Aldrich (St. Louis, MO, USA). Sodium chloride (NaCl), isopropanol, and glycerol were purchased from J.T. Baker Chemicals (Phillipsburg, NJ, USA); hydrochloric acid (HCl) from AmericanBio (Natick, Massachusetts, USA); and sodium hydroxide (NaOH) from Avantor (Center Valley, Pennsylvania, USA). Silicon wafers (Mechanical Grade 1996) were provided by UniversityWafer, Inc. (South Boston, MA, USA). Deionized (DI) water (MilliPore, Billerica, MA, USA) was used for solution preparation, membrane compaction, and cleaning the filtration system.

2.2. Fabrication of NF membranes by LbL assembly

Before deposition of the PEs onto the PSf UF membrane substrate, the PSf membrane was immersed in 25% isopropanol and shaken at 60 rpm for 30 min, followed by thorough rinsing with DI water in three 30-min cycles. The pretreated PSf membrane was stored in DI water at 4°C overnight before use. For LbL assembly, the pretreated PSf membrane was clamped between a glass plate and a polytetrafluoroethylene (PTFE) frame with the active side facing up (the exposed membrane area was approximately 40 cm^2) [6,47]. The frame was placed on a rotary shaker, which was set to 60 rpm, and then 10 mL of cationic and anionic PE solutions were deposited onto the PSf membrane in an alternating fashion with intermediate rinsing cycles. PDADMAC and PSS were chosen as cationic and anionic PEs, respectively, because they are both charged over the normal operational pH [8,37].

The PE concentration of the deposition solutions used was either 0.8 or 20 mM, calculated with respect to the monomer molar mass. The PE

concentration was decreased to fabricate membranes with smaller pore sizes, as described in our previous work [6]. In both cases, the PEs were dissolved in DI water with 0.5 M NaCl as the background ionic strength, and a 0.5 M NaCl solution was used for rinsing. As the pristine PSf membrane has a negative surface zeta potential (Fig. S2), LbL assembly was initiated by the deposition of cationic PDADMAC onto the substrate. The PSf membrane was exposed to the PDADMAC solution for 10 min, followed by two 5-min rinsing cycles to remove any loosely adsorbed PDADMAC. Subsequently, the PSS solution was applied to the substrate for 10 min, followed by two 5-min rinsing cycles. These six steps concluded the first bilayer. PEM NF membranes with four, seven, and ten bilayers were fabricated to produce PEM NF membranes of different thicknesses. The subsequent bilayers were fabricated in a similar manner as described above, except for the top bilayer, where salt annealing was introduced [53,55]. The PEM was annealed by applying 10 mL of 2 M NaCl for 30 min to the membrane prior to depositing the terminating PSS layer. After LbL assembly, the PEM NF membranes were immersed in 15% wt. glycerol for 4 h, and then air-dried overnight at room temperature. The membranes were thoroughly rinsed with DI water before use.

2.3. NF system, water flux and solute rejection measurements

Filtration experiments were conducted in a bench-scale crossflow system, with flat-sheet membranes placed in plate-and-frame cells. The effective membrane surface area was 20.02 cm^2. Feed solution recirculated between the membrane cells and a feed tank at a crossflow velocity of 0.21 m s^{-1}. The temperature of the feed solution was controlled by a heater/chiller system (±1 °C). The membranes were compacted overnight at high pressure—9.7 bar (140 psi) before filtrations of salt solutions and 13.8 bar (200 psi) before filtrations of organic solutions—using DI water. Pure water flux was measured gravimetrically at the beginning of each experiment and then a concentrated stock solution was added to the feed tank to reach either 4 mM NaF/NaBr or 50 mg L^{-1} total organic carbon (TOC) (glucose/erythritol/xylose). Additionally, filtration of a mixed anion solution containing 2 mM of each NaCl, NaF, and NaBr was conducted. Filtrations of salt solutions were conducted at 1.7, 5.2, and 6.9 bar (25, 75, and 100 psi), and at 22, 28, 34, and 40 °C for each operational pressure. Filtrations of organic solutions were conducted at 4.1, 6.2, 8.3, and 10.3 bar (60, 90, 120, and 150 psi), and 25 °C. The system was stabilized for 30 min at each pressure and temperature, after which samples of the feed and permeate were collected to determine membrane water flux (gravimetrically) and solute rejection. Ion concentration of single salt solutions was measured using an electrical conductivity meter (Oakton Instruments, Vernon Hills, IL, USA) and mixed salt solutions were measured with ion chromatography (Dionex DX-500 with an AS14A IonPac column). Organic concentration was measured using a TOC analyzer (TOCV-CSH, Shimadzu Corp., Japan). The observed rejection, R_{obs}, was calculated using the equation:

$$R_{obs} = \left(1 - \frac{c_p}{c_f}\right) \times 100\% \quad (1)$$

where c_p and c_f are the solute concentrations of the permeate and feed, respectively. Water permeability of the PEM NF membranes was calculated from water flux measured during filtrations of 4 mM NaBr at 22 °C, and at 1.7, 5.2, and 6.9 bar (25, 75, and 100 psi).

2.4. Membrane characterization

PEM film thickness was evaluated using atomic force microscopy (AFM). For this purpose, the PEM films were fabricated on atomically smooth silicon wafers, with 1 mL of PE and rinse solutions applied to the substrate using small PTFE frames. Similar to the procedure described in Section 2.2, the PEM films were formed by alternating deposition of PDADMAC and PSS to the substrate for 10 min, with two 5-min intermediate rinsing cycles, and salt annealing to the terminating bilayer. The PEM samples were rinsed with DI water and air-dried overnight. Before AFM scanning, the dry PEM films were scratched with a needle without damaging the silicon wafer. PEM samples were measured using a Bruker Dimension FastScan AFM (Santa Barbara, CA, USA) equipped with a Bruker FastScan-B cantilever (5 nm tip radius) in ScanAsyst mode. AFM images of the edge of the scratch were captured at a scan rate of 3 Hz. Height profiles across the scratch were obtained by an image analysis software, NanoScope Analysis v1.9 (Bruker), using the section tool. The height difference between the PEM film and the bare silicon wafer revealed the dry PEM film thickness. PEM thicknesses are reported as the average and standard deviation of six measurements (three scratches on two PEM films). Statistical difference was assessed using one-way ANOVA and the results are reported as *p*-values.

An estimation of the average pore size of the PEM NF membranes was calculated using the hydrodynamic pore transport model [56]. The model assumes the membrane to be a bundle of cylindrical capillary tubes of constant radii and uses rejection data of neutral organic solutes for the pore size estimation, as was described previously by our group [6,18,57]. Solute flux and rejection data for erythritol (MW 122 g mol^{-1}), xylose (MW 150 g mol^{-1}) and glucose (MW 180 g mol^{-1}) were collected during single solute filtrations using the crossflow system, filtration conditions, and analytical methods described in Section 2.3. These data were fed to the hydrodynamic pore transport model, and the average membrane pore radius was estimated from transport data for each organic solute. Estimated pore sizes and standard deviations are reported based on the results obtained from erythritol, xylose and glucose rejections. Statistical difference was assessed using one-way ANOVA and the results are reported as *p*-values. The model has been described in detail by Deen [56] and Nghiem et al. [57], and a short description of the method is provided in the Supplementary Material.

The surface zeta potential of the PEM NF membranes was calculated from streaming potential measurements using an electro-kinetic analyzer with an asymmetric clamping cell (EKA, Brookhaven Instruments, Holtsville, NY, USA) as described elsewhere [8,14]. The surface zeta potential was determined at pH 5, 7, and 9 using a constant background electrolyte concentration of 1 mM KCl and 0.1 mM $KHCO_3$. PEM NF membranes were prepared on PSf UF substrate by the method described in Section 2.2, except using a bigger PTFE frame and 20 mL of PE and rinse solutions. The results are reported as the average and standard deviation of two independent samples, with eight streaming potential measurements per sample.

2.5. Determination of energy barriers to ion transport

Experimental energy barriers to ion transport through the PEM NF membranes were determined from an Arrhenius-type equation:

$$J_s = A\ exp\left(-\frac{E_a}{RT}\right) \quad (2)$$

where J_s is the ion flux through the membrane, A is a pre-exponential factor, E_a is the experimental energy barrier, R is the universal gas constant, and T is the absolute temperature. A linearized form of Eq. (2) describes the natural logarithm of ion flux through the membrane as a function of the inverse of the absolute temperature:

$$\ln J_s = \ln A - \frac{E_a}{RT} \quad (3)$$

Energy barriers to ion transport through the PEM NF membranes were calculated from the slope of the line resulting from Eq. (3). The ion flux, J_s, was calculated at different feed temperatures from experimental data according to:

$$J_s = J_w c_p \quad (4)$$

where J_w is the water flux through the membrane and c_p is the ion concentration in the permeate. The ion flux was normalized to the feed concentration at each sampling to eliminate any effect of feed concentration variability due to sampling and solvent evaporation at elevated temperatures. Energy barriers to water transport were calculated in a similar manner as for ion transport, except using water flux instead of solute flux in Eq. (3).

Water flux and rejection data for fluoride, bromide, and chloride were collected in single and mixed sodium salt filtrations, using the crossflow system, filtration conditions, and analytical methods described in Section 2.3. The experimental energy barriers to water and ion transport in the PEM NF membranes with four, seven, and ten bilayers were calculated from these data. The average and standard deviation are reported from at least three independently fabricated membranes. Statistical difference was assessed using one-way ANOVA and Welch two-sample *t*-tests, and the results are reported as *p*-values.

3. Results and discussion

3.1. Characterization of PEM NF membranes

The aim of this study was to investigate the effect of intra-pore ion transport on energy barriers in NF membranes. To do so, we fabricated PEM NF membranes of different thicknesses by changing the number of bilayers of PDADMAC/PSS deposited on a PSf UF substrate. The PEM fabrication conditions were selected so that only the thickness of the PEM NF membranes changed by addition of bilayers, while changes in membrane pore size and surface charge were minimized. We estimated the PEM thickness, average pore size, and surface zeta potential using AFM, the hydrodynamic pore transport model, and an electro kinetic analyzer, respectively, to quantify variations in these membrane properties.

For thickness measurements, PEMs with four, seven, and ten bilayers of PDADMAC/PSS were fabricated on atomically smooth silicon wafers. After assembly, the PEM films were dried and then scratched with a needle before imaging with AFM (Fig. S1). A scan of the edge of the scratch revealed the height difference between the PEM and the bare silicon wafer, which corresponded to the dry PEM thickness (Fig. 1A–C). The PEM thickness increased from 28 to 77 nm for PEMs with four to ten bilayers ($p < 0.001$, Fig. 1C). The observed PEM film growth was linear with an average bilayer thickness of 7.9 nm, which is in good agreement with results reported elsewhere for similar systems [6,50,52,58]. The measured PEM thickness indicates the increase in thickness of the separation layers of the PEM NF membranes with addition of bilayers, although the thickness may not be directly comparable to the PEMs on porous UF membranes. When PEMs are assembled on porous substrates, the PEM growth begins in a pore regime (filling of the pores) before it reaches the film regime (increasing film thickness) [50,53]. Here, we deposited at least four bilayers onto the PSf UF substrate to be within the film regime across all experiments.

The average pore sizes of the PEM NF membranes were estimated using the hydrodynamic pore transport model. Membranes with four, seven, and ten bilayers of PDADMAC/PSS were fabricated on PSf UF substrates and applied in filtrations of neutral organic solutes (erythritol, xylose, and glucose). The pore size calculations were based on rejection data for the solutes (Table S2), as described elsewhere [6,57]. Pore sizes were seemingly not affected by the number of bilayers in the PEM films, as the average estimated pore radii were calculated to be 0.73, 0.70, and 0.74 nm for the PEM NF membranes with four, seven, and ten bilayers, respectively ($p = 0.76$, Fig. 1C). Similarly, the variation in surface zeta potential among the PEM NF membranes with different number of bilayers was small and assumed not to affect the energy barrier measurements (Fig. 1D). The control over surface charge was achieved by applying salt annealing to the PEM NF membranes during fabrication. Preliminary experiments showed that the surface zeta potential of PEM NF membranes with two, four, and eight bilayers of PDADMAC/PSS fabricated without salt annealing became increasingly positive with addition of bilayers, even with PSS (anionic) as the terminating PE (Fig. S2). This phenomenon has been commonly explained by overcompensation of PDADMAC in the PEM due to an uneven adsorption of PDADMAC and PSS to the film, which results in accumulation of excess PDADMAC with addition of bilayers [51,53,58]. Salt annealing has been proposed as a method to restore the stoichiometric balance between PDADMAC and PSS in PEM films [55]. Briefly, the mobility of the PEs within the PEM is enhanced by exposure to high salt concentration (>1.5 M NaCl), whereby the excess, extrinsic PDADMAC sites (charge-neutralized by salt counter-ions from the deposition solution) are evenly dispersed through the PEM, allowing a higher uptake of PSS at the surface in the following deposition cycle [55]. By applying salt annealing, we were able to produce membranes with different number of bilayers but similar, negative surface charges (Fig. 1D).

The filtration performance of the PEM NF membranes (water permeability and solute rejection, Table 1) supports the results obtained from characterization. Water permeability decreased from 9.01 to 6.61 L m^{-2} h^{-1} bar^{-1} upon increasing the number of bilayers from four to ten ($p < 0.01$), which can be explained by higher resistance to water flux in thicker membranes [12]. Notably, the decrease in water flux was not inversely proportional to the increase in membrane thickness, which indicates that partitioning into the membrane imposed a higher resistance to transport than diffusion inside the membrane [38]. Glucose and bromide rejection remained similar for the three membranes ($p > 0.57$ for both solutes), which is in agreement with results from the hydrodynamic pore transport model and electro kinetic analyzer, respectively. The similarity in the rejection values is also consistent with predictions of a pore transport model proposed by Bowen and Welfoot [59], who showed that rejection of uncharged solutes and ions is independent of membrane thickness.

Membrane thickness increased significantly with the addition of bilayers to the PEMs while pore size and surface zeta potential were comparatively unaffected (Fig. 1). The similarity in pore size was particularly important for measurements of energy barriers to ion transport through the membranes, given the reported effect of steric hindrance on ion dehydration (i.e., greater need for ion dehydration when ions pass through smaller membrane pores) [25]. Thus, the characterization proves the usefulness of the PEM NF membranes for studying the effect of membrane thickness on energy barriers to ion transport in NF membranes.

3.2. Effects of membrane thickness on apparent energy barriers to ion transport

We applied PEM NF membranes of varying thicknesses (with four, seven, and ten bilayers of PDADMAC/PSS) in filtrations of ionic solutions and calculated the energy barriers to ion transport through the membranes, according to the linearized Arrhenius equation (Eq. (3)). In an attempt to limit the dominating effect of ion dehydration at the pore

Table 1
Water permeability and solute rejection of PEM NF membranes.

	4 Bilayers 20 mM PE	7 Bilayers 20 mM PE	10 Bilayers 20 mM PE
Water permeability[a] (L m^{-2} h^{-1} bar^{-1})	9.01 ± 1.13	8.46 ± 0.91	6.61 ± 0.47
Bromide rejection, R_{obs}[b] (%)	16.3 ± 4.2	12.9 ± 3.2	17.9 ± 2.7
Glucose rejection, R_{obs}[c] (%)	39.6 ± 10.1	43.5 ± 4.5	43.2 ± 2.1

[a] Filtration of bromide solution (4 mM NaBr), at 22 °C, pH 5.7, and 1.7, 5.2, and 6.9 bar.
[b] Measured at 22 °C, 6.9 bar, and pH 5.7, feed concentration 4 mM NaBr.
[c] Measured at 25 °C, 6.2 bar, and pH 5.7, feed concentration 50 mg L^{-1} TOC.

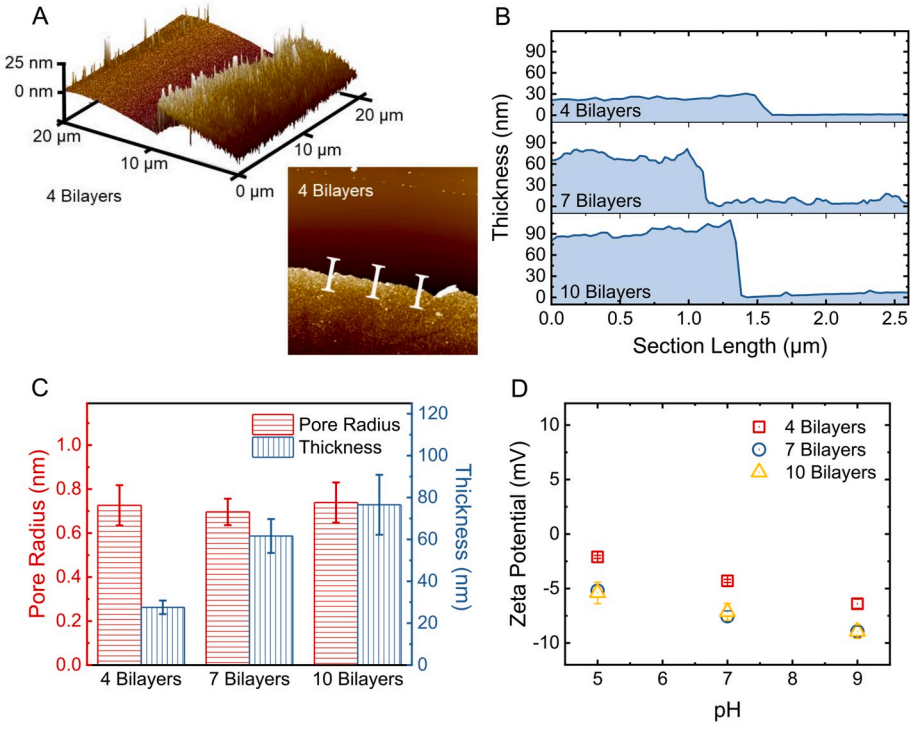

Fig. 1. Characterization of PEM films and PEM NF membranes prepared with four, seven, and ten bilayers using 20 mM PDADMAC/PSS deposition solutions. (A) Sample AFM images (20 × 20 μm, 3-D and 2-D) of a dry PEM film with four bilayers of PDADMAC/PSS on a silicon wafer. Before imaging, a scratch was generated by dragging a needle across the dry PEM film. The images show the topology of the PEM film and the bare silicon wafer around one edge of the scratch. (B) Sample height profiles of PEM films obtained from AFM. The thickness of the PEM films was calculated from the height profiles as the difference in height between the PEM film (thicker part) and the bare silicon wafer (thinner part). Three different scratches on two independent coupons were measured. (C) Average estimated pore size ($p = 0.76$) and thickness ($p < 0.001$) of PEM NF membranes and films, respectively. PEM NF membranes were fabricated on PSf UF substrate. Pore size was determined from the hydrodynamic pore transport model, using rejection of erythritol, xylose, and glucose in single-solute filtration experiments at applied pressures of 4.1, 6.2, 8.3, and 10.3 bar (60, 90, 120, and 150 psi). Experimental conditions: feed concentration 50 mg L^{-1} TOC, crossflow velocity 0.21 m s^{-1}, and temperature 25 °C. (D) Surface zeta potential of PEM NF membranes fabricated on PSf UF substrate. The surface zeta potential was calculated from eight streaming potential measurements on two independent coupons using a constant background electrolyte concentration of 1 mM KCl and 0.1 mM $KHCO_3$. The pH was adjusted using hydrochloric acid (HCl) and sodium hydroxide (NaOH). (For interpretation of the references to colour in this figure legend, the reader is referred to the Web version of this article.)

entry on the apparent energy barrier, we used bromide ions with relatively low hydration energy and PEM NF membranes with average pore sizes larger than the hydrated size of the ions in our study. By using such a system, the potential effect of membrane thickness, i.e., the contribution of the transport resistance arising within the membrane, on the apparent energy barrier should have become more evident.

Bromide flux through the membranes was measured at temperatures ranging from 22 to 40 °C and operating pressures of 1.7–6.9 bar (Fig. 2). An increase in the two operating parameters led to an increase in bromide flux. Generally, solute flux increases at higher pressure (up to a certain critical pressure) mostly due to enhanced convective flow [25,60], while higher temperature leads to increased diffusion, decreased water viscosity, and potentially altered membrane pore structure (e.g., due to fusion of adjacent pores) [61–63]. The effect of temperature on the PEM pore sizes and water viscosity was investigated by comparing the calculated energy barriers for water and ion transport through the membranes (Fig. S3). The energy barriers for water were always lower than for ions, so the observed increase in bromide flux at higher temperatures cannot be explained entirely by increased pore size or decreased water viscosity. Rather, an additional ion-specific mechanism (i.e., ion dehydration) was involved in bromide transport in addition to convection, which resulted in higher energy barriers to bromide transport than water transport. The relatively small difference between the energy barriers for water and bromide transport (especially in the membranes with larger pore size) suggests, however, that bromide transport through the membranes was significantly affected by convection. In addition to the influence of pressure and temperature, bromide flux decreased with membrane thickness, which can be explained by increased resistance to convective and diffusive transport [12]. However, the reduction in bromide flux was comparatively lower than the increase in membrane thickness, suggesting that hindrance to transport was composed of another major barrier than intra-pore diffusion, such as ion dehydration at the solution-membrane interface.

Arrhenius plots were produced from bromide fluxes at different temperatures by plotting the natural logarithm of the bromide flux against the inverse of the absolute temperature (Fig. 3A). The linearity of the Arrhenius plots verifies the occurrence of thermally activated transport through the membranes, and the slopes of the Arrhenius plots were thus used to calculate the apparent energy barriers (Fig. 3B) [38]. The energy barriers to bromide transport in PEM NF membranes of different thicknesses ranged from 3.4 to 4.4 kcal mol^{-1}; these barriers are comparable to energy barriers calculated elsewhere for commercial NF and ion-exchange membranes [22,37]. Notably, the data do not show a relationship between the energy barriers and membrane thickness. More specifically, the energy barriers do not increase with increased membrane thickness, suggesting that the apparent energy barrier is not an accumulative parameter with respect to membrane thickness; instead, it represents the local energy barrier of the rate-limiting step. Our results thus support previously published models on diffusion in membranes describing solute transport as sequential (and local) barriers in series, rather than a single accumulative barrier over the membrane [38].

Similar observations have been described previously by Epsztein et al. [22,37] who found energy barriers to ion transport in ion-exchange membranes to be comparable to those for NF membranes, despite ion-exchange membranes being much thicker than NF membranes. The authors concluded that the energy barriers were mainly due to ion dehydration at the pore entry, in agreement with previous studies [22,25,46]. According to transport models based on the transition-state theory [38], if the energy barrier due to intra-pore diffusion is significant, solute flux will depend inversely on membrane thickness. Here, the relatively minor effect of thickness on solute flux (Fig. 2) suggests that the barrier at the solution-membrane interface is the rate-limiting step and therefore poses the most significant barrier for solute transport.

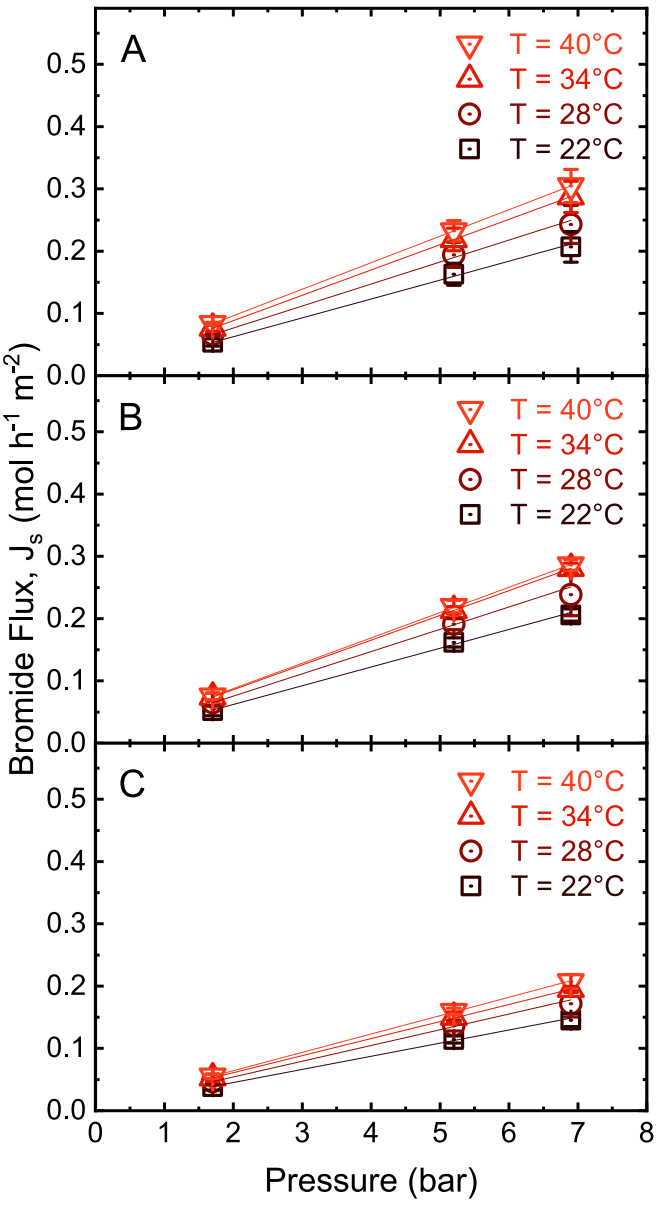

Fig. 2. Bromide flux through PEM NF membranes with (A) four, (B) seven, and (C) 10 bilayers of PDADMAC/PSS. Membranes were prepared by deposition of 20 mM polyelectrolyte solutions onto a PSf UF substrate. Bromide flux was measured during filtration of 4 mM NaBr solutions at 1.7, 5.2, and 6.9 bar (25, 75, and 100 psi). Rejection was calculated from conductivity measurements of the feed and permeate. Experimental conditions: crossflow velocity of 0.21 m s^{-1}, pH 5.7. Error bars report standard deviations of four independently fabricated membranes.

Although the average pore size was relatively large in our experiments and transport was dominated by convection rather than diffusion, some pores may still force bromide ions to partially dehydrate or, at least, rearrange their hydration shells at the pore entrance.

3.3. Effect of hydration energy, pore size, and pressure on apparent energy barriers to ion transport

To verify that ion dehydration governs the apparent energy barrier, we studied the effects of ion hydration energy and membrane pore size on energy barriers to ion transport in PEM NF membranes. We fabricated PEM NF membranes with different pore sizes by varying the concentrations of PEs in the deposition solutions from 0.8 to 20 mM, which resulted in membranes with average estimated pore radii of 0.62 and 0.70 nm, respectively, as estimated from the hydrodynamic pore transport model. We then determined the energy barriers to bromide transport through those membranes (Fig. 4B). The effect of ion hydration energy on energy barriers was investigated by comparing bromide and fluoride transport (hydration energies of 75.3 and 111.1 kcal mol^{-1}, respectively [22]) in PEM NF membranes with seven bilayers of PDADMAC/PSS and an average estimated pore radius of 0.62 nm (Fig. 4A).

Both higher ion hydration energy (fluoride) and smaller membrane pore size (0.8 mM PE) resulted in increased energy barriers to ion transport through the PEM NF membranes (Fig. 4 and Fig. S4), in contrast to increased membrane thickness (Fig. 3B). As such, hydration energy and pore size had a greater effect on energy barriers than membrane thickness, which suggests that partial ion dehydration controls the apparent energy barrier to ion transport in NF membranes. Welch two-sample *t*-tests showed significant differences in energy barriers for bromide and fluoride ions ($p = 0.01$–0.05) as well as for the pore sizes ($p = 0.02$–0.16), where the *p*-values vary depending on the applied pressure. Larger differences may have been observed in membranes with pore sizes more comparable to the hydrated size of the ions, where diffusive transport is relatively more important in comparison to convective transport.

Energy barriers to ion transport in membranes have been found to decrease to some extent upon increasing the operating pressure, notably when the ions experience a high resistance to partitioning into the membrane due to high ion hydration energy and narrow pores [25]. Considering that the apparent energy barrier is calculated from the Arrhenius-type equation where solute flux is described as a function of temperature, the decrease in energy barriers at higher pressure (or higher water permeation velocity) may be the result of increased contribution of convective transport over diffusive transport at higher pressure [1,20]. The temperature dependence of diffusion thereby becomes comparatively less important for solute flux, which can be observed as a decrease in the apparent energy barrier at higher pressure. We evaluated the effects of pressure on the energy barriers and found that pressure effects were generally not apparent, with the exception of fluoride transport through the denser membrane studied (pore radius of 0.62 nm, Fig. 4A). The pressure effect was thus more pronounced as the need for ion dehydration was higher, in agreement with reported observations [25,62]. The energy barrier to fluoride transport decreased significantly with pressure ($p < 0.001$), while no pressure effects on the energy barriers to bromide transport were observed at the operating pressures applied here, suggesting that bromide transport was largely convection-controlled. Based on these observations, pressure may potentially be exploited to tune the selectivity of NF membranes towards ions of similar hydrated size and charge.

3.4. Mechanisms of ion transport through PEM NF membranes

The apparent energy barrier to solute transport in membranes was originally described by a membrane diffusion model derived from the transition-state theory [38]. According to this model, the apparent energy barrier is dependent on both the energy barriers to intra-pore diffusion and the energy barrier due to solute partitioning into the membrane. Similarly, the transport of ions through a PEM NF membrane may be described as a sequence of energy barriers that arise due to ion partitioning into the membrane pores and diffusion across the membrane thickness (Fig. 5) [38,64]. Although the apparent energy barrier theoretically depends on both steps, it is governed by the rate-limiting step during transport, or the step that imposes a higher energy barrier [38]. We found that membrane thickness did not affect the apparent energy barriers calculated here, indicating that the apparent energy barrier is not an accumulative parameter with respect to thickness. Instead, the apparent energy barrier represents a single local barrier as described by the membrane diffusion model [38]. Notably, the relatively

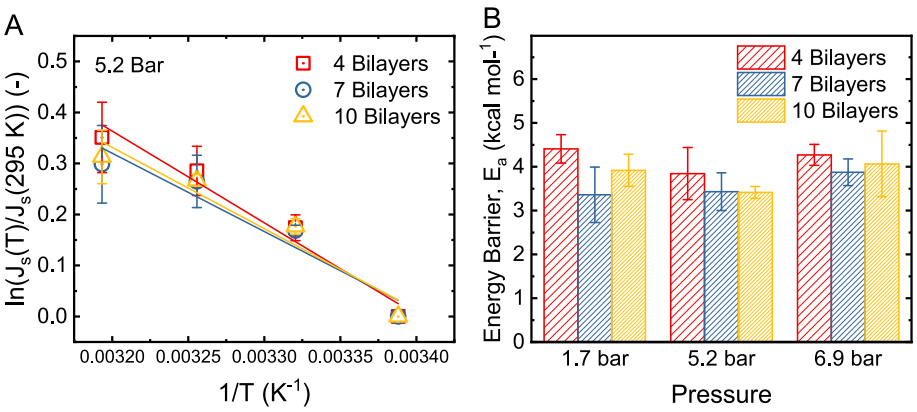

Fig. 3. (A) Arrhenius plots and (B) experimental energy barriers to bromide transport through PEM NF membranes with four, seven, and ten bilayers of PDADMAC/PSS. Membranes were prepared by deposition of 20 mM PE solutions onto a PSf UF substrate. (A) Bromide flux was determined during filtration of 4 mM NaBr at 22, 28, 34, and 40 °C; 5.2 bar (75 psi); crossflow velocity of 0.21 m s^{-1}; and pH 5.7. The bromide flux was normalized to the flux at 22 °C (295 K) and the natural logarithm of the normalized flux was plotted against the inverse of the absolute temperature, according to the linearized Arrhenius equation. (B) Energy barriers were calculated from the slopes of the Arrhenius plots at applied pressures of 1.7, 5.2, and 6.9 bar (25, 75, and 100 psi), under the same conditions as in (A) ($p = 0.23$, 0.41, and 0.32 for 1.7, 5.2, and 6.9 bar, respectively). Error bars report standard deviations of four independently fabricated membranes.

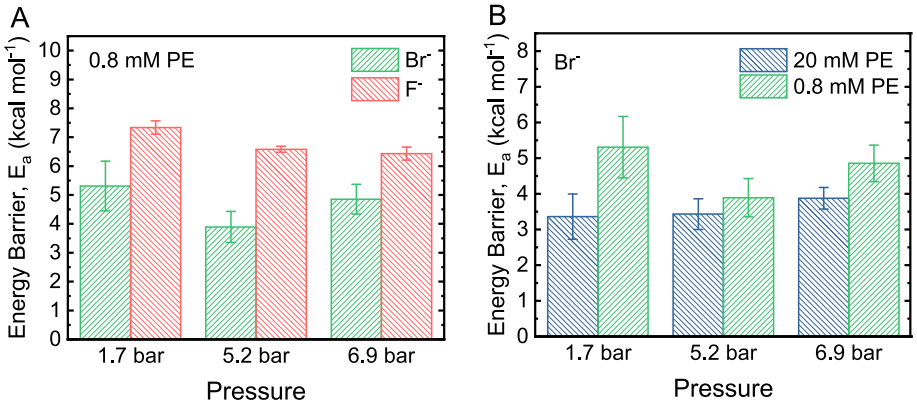

Fig. 4. (A) Experimental energy barriers to transport of anions of different hydration energies (Br^- = 75.3 kcal mol^{-1}; F^- = 111.1 kcal mol^{-1}) through PEM NF membranes with seven bilayers of PDADMAC/PSS (Welch two-sample *t*-tests; p = 0.05, 0.01, and 0.02 for 1.7, 5.2, and 6.9 bar, respectively). Membranes were prepared by deposition of 0.8 mM PE solutions onto a PSf UF substrate. (B) Experimental energy barriers to bromide transport through PEM NF membranes of different pore sizes (Welch two-sample *t*-tests; p = 0.02, 0.16, and 0.03 for 1.7, 5.2, and 6.9 bar, respectively). PEM NF membranes were prepared by deposition of seven bilayers of 20 mM (pore radius = 0.70 nm) and 0.8 mM (pore radius = 0.62 nm) PDADMAC/PSS onto a PSf UF substrate. The energy barriers were calculated from flux and rejection data from filtration of single salt solutions (4 mM NaBr or 4 mM NaF) at 22, 28, 34, and 40 °C; crossflow velocity of 0.21 m s^{-1}; and pH 5.7. The energy barriers were calculated from the slope of Arrhenius plots, where the natural logarithm of ion flux through the membranes was plotted against the inverse of the absolute temperature. Error bars report standard deviations of three independently fabricated membranes.

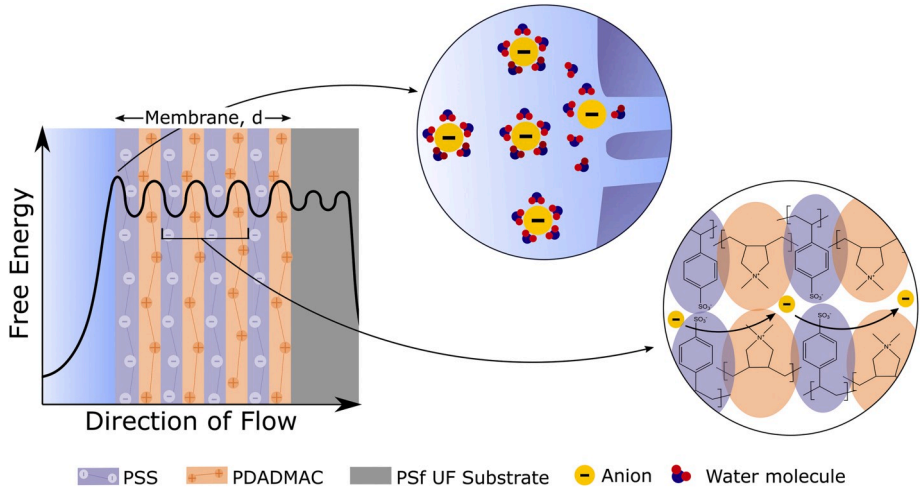

Fig. 5. Schematic description of energy barriers to anion transport through PEM NF membranes. The main energy barrier arises at the membrane-water interface, where ions undergo dehydration, or deformation of their hydration shells, before they enter the pore. The ions overcome further energy barriers as they move through the membrane and hop between vacant sites and between charged groups of the membrane.

small effect of thickness on ion flux, even with the local charge stabilization of the dehydrated ion during diffusion through the membranes, suggests that transport was mainly controlled by ion partitioning into the membrane, i.e. ion dehydration at the solution-membrane interface, and not by diffusion inside the membrane.

While ion rejection and the apparent energy barriers to ion transport were unaffected by increasing membrane thickness, water permeability and solute flux decreased to some extent due to a greater resistance to water transport. Membrane thickness thus somewhat influenced the rate of transport through the membranes but did not play a role in ion selectivity. The selectivity of the membranes was solely dictated by the pore size of the membrane and properties of the ions. Once a solute has crossed the largest energy barrier at the pore entry, the solute traverses the membrane without being significantly affected by the pore interior [38].

4. Conclusion

We investigated the role of intra-pore diffusion in the apparent energy barriers to ion transport in NF membranes. PEM NF membranes were prepared using PE LbL assembly, where one membrane property (either membrane thickness or pore size) was varied while other membrane properties were kept constant. The apparent energy barriers to bromide and fluoride transport through the membranes were calculated from an Arrhenius-type equation. We found no distinguishable effect on the apparent energy barriers to bromide transport when changing membrane thickness, whereas both ion hydration energy and membrane pore size significantly affected the apparent energy barriers. The results indicate that the apparent energy barriers to ion transport were mainly controlled by ion dehydration at the water-membrane interface (i.e., in entering or partitioning into the pore) rather than intra-pore diffusion. This observation was supported by predictions of a membrane diffusion model previously derived from the transition-state theory, which shows that solute permeation (translated to the apparent energy barrier here) is independent of membrane thickness when transport is controlled by partitioning of the solute into the membrane. The results highlight the important role of ion dehydration at the water-membrane interface in controlling ion rejection by NF membranes and simultaneously eliminate membrane thickness as a parameter involved in ion dehydration-based selectivity.

Declaration of competing interest

The authors declare that they have no known competing financial interests or personal relationships that could have appeared to influence the work reported in this paper.

CRediT authorship contribution statement

Sigyn B. Sigurdardottir: Conceptualization, Methodology, Formal analysis, Investigation, Writing - original draft, Writing - review & editing, Visualization. **Ryan M. DuChanois:** Conceptualization, Methodology, Investigation, Writing - original draft, Writing - review & editing. **Razi Epsztein:** Conceptualization, Methodology, Investigation, Writing - original draft, Writing - review & editing, Supervision. **Manuel Pinelo:** Supervision, Funding acquisition, Writing - review & editing. **Menachem Elimelech:** Resources, Supervision, Funding acquisition, Writing - review & editing.

Acknowledgements

This work was supported by The Danish Council for Independent Research, Grant no.: 6111-00232B. In addition, we acknowledge the support received from the National Science Foundation (NSF) through the Engineering Research Center for Nanotechnology-Enabled Water Treatment (EEC-1449500). Facilities used for AFM were supported by the Yale Institute of Nanoscale and Quantum Engineering (YINQE) under NSF MRSEC DMR 1119826. We also acknowledge the NSF Graduate Research Fellowship awarded to R.M.D. and the postdoctoral fellowship (to R. E.) provided from the United States-Israel Binational Agricultural Research and Development (BARD) Fund, Fellowship Number FI-549-2016.

Appendix A. Supplementary data

Supplementary data to this article can be found online at https://doi.org/10.1016/j.memsci.2020.117921.

References

[1] J. Luo, Y. Wan, Effect of highly concentrated salt on retention of organic solutes by nanofiltration polymeric membranes, J. Membr. Sci. 372 (2011) 145–153, https://doi.org/10.1016/j.memsci.2011.01.066.
[2] N. Hilal, H. Al-Zoubi, N.A. Darwish, A.W. Mohammad, M. Abu Arabi, A comprehensive review of nanofiltration membranes: treatment, pretreatment, modelling, and atomic force microscopy, Desalination 170 (2004) 281–308, https://doi.org/10.1016/j.desal.2004.01.007.
[3] N.N. Bui, M.L. Lind, E.M. V Hoek, J.R. McCutcheon, Electrospun nanofiber supported thin film composite membranes for engineered osmosis, J. Membr. Sci. (2011) 385–386, https://doi.org/10.1016/j.memsci.2011.08.002, 10–19.
[4] B. Tansel, J. Sager, T. Rector, J. Garland, R.F. Strayer, L. Levine, M. Roberts, M. Hummerick, J. Bauer, Significance of hydrated radius and hydration shells on ionic permeability during nanofiltration in dead end and cross flow modes, Separ. Purif. Technol. 51 (2006) 40–47, https://doi.org/10.1016/j.seppur.2005.12.020.
[5] J.R. Werber, C.O. Osuji, M. Elimelech, Materials for next-generation desalination and water purification membranes, Nat. Rev. Mater. 1 (2016) 16018, https://doi.org/10.1038/natrevmats.2016.18.
[6] R.M. DuChanois, R. Epsztein, J.A. Trivedi, M. Elimelech, Controlling pore structure of polyelectrolyte multilayer nanofiltration membranes by tuning polyelectrolyte-salt interactions, J. Membr. Sci. 581 (2019) 413–420, https://doi.org/10.1016/j.memsci.2019.03.077.
[7] R. Epsztein, W. Cheng, E. Shaulsky, N. Dizge, M. Elimelech, Elucidating the mechanisms underlying the difference between chloride and nitrate rejection in nanofiltration, J. Membr. Sci. 548 (2018) 694–701, https://doi.org/10.1016/j.memsci.2017.10.049.
[8] W. Cheng, C. Liu, T. Tong, R. Epsztein, M. Sun, R. Verduzco, J. Ma, M. Elimelech, Selective removal of divalent cations by polyelectrolyte multilayer nanofiltration membrane: role of polyelectrolyte charge, ion size, and ionic strength, J. Membr. Sci. 559 (2018) 98–106, https://doi.org/10.1016/j.memsci.2018.04.052.
[9] I. Koyuncu, D. Topacik, Effect of organic ion on the separation of salts by nanofiltration membranes, J. Membr. Sci. 195 (2002) 247–263, https://doi.org/10.1016/S0376-7388(01)00559-2.
[10] L.S. White, A.R. Nitsch, Solvent recovery from lube oil filtrates with a polyimide membrane, J. Membr. Sci. 179 (2000) 267–274, https://doi.org/10.1016/S0376-7388(00)00517-2.
[11] J. Luo, Y. Wan, Effects of pH and salt on nanofiltration-a critical review, J. Membr. Sci. 438 (2013) 18–28, https://doi.org/10.1016/j.memsci.2013.03.029.
[12] B. Su, T. Wang, Z. Wang, X. Gao, C. Gao, Preparation and performance of dynamic layer-by-layer PDADMAC/PSS nanofiltration membrane, J. Membr. Sci. (2012) 423–424, https://doi.org/10.1016/j.memsci.2012.08.041, 324–331.
[13] R. Zhang, Y. Su, X. Zhao, Y. Li, J. Zhao, Z. Jiang, A novel positively charged composite nanofiltration membrane prepared by bio-inspired adhesion of polydopamine and surface grafting of poly(ethylene imine), J. Membr. Sci. 470 (2014) 9–17, https://doi.org/10.1016/j.memsci.2014.07.006.
[14] Y.C. Chiang, Y.Z. Hsub, R.C. Ruaan, C.J. Chuang, K.L. Tung, Nanofiltration membranes synthesized from hyperbranched polyethyleneimine, J. Membr. Sci. 326 (2009) 19–26, https://doi.org/10.1016/j.memsci.2008.09.021.
[15] D. Menne, C. Üzüm, A. Koppelmann, J.E. Wong, C. van Foeken, F. Borre, L. Dähne, T. Laakso, A. Pihlajamäki, M. Wessling, Regenerable polymer/ceramic hybrid nanofiltration membrane based on polyelectrolyte assembly by layer-by-layer technique, J. Membr. Sci. 520 (2016) 924–932, https://doi.org/10.1016/j.memsci.2016.08.048.
[16] J. De Grooth, D.M. Reurink, J. Ploegmakers, W.M. De Vos, K. Nijmeijer, Charged micropollutant removal with hollow fiber nanofiltration membranes based on polycation/polyzwitterion/polyanion multilayers, ACS Appl. Mater. Interfaces 6 (2014) 17009–17017, https://doi.org/10.1021/am504630a.
[17] S.T. Morthensen, S.B. Sigurdardottir, A.S. Meyer, H. Jørgensen, M. Pinelo, Separation of xylose and glucose using an integrated membrane system for enzymatic cofactor regeneration and downstream purification, J. Membr. Sci. 523 (2017) 327–335, https://doi.org/10.1016/j.memsci.2016.10.017.
[18] C. Boo, Y. Wang, I. Zucker, Y. Choo, C.O. Osuji, M. Elimelech, High performance nanofiltration membrane for effective removal of perfluoroalkyl substances at high water recovery, Environ. Sci. Technol. 52 (2018) 7279–7288, https://doi.org/10.1021/acs.est.8b01040.
[19] A.W. Mohammad, Y.H. Teow, W.L. Ang, Y.T. Chung, D.L. Oatley-Radcliffe, N. Hilal, Nanofiltration membranes review: recent advances and future prospects, Desalination 356 (2015) 226–254, https://doi.org/10.1016/j.desal.2014.10.043.

[20] S. Bhattacharjee, J.C. Chen, M. Elimelech, Coupled model of concentration polarization and pore transport in crossflow nanofiltration, AIChE J. 47 (2001) 2733–2745, https://doi.org/10.1002/aic.690471213.

[21] S.U. Hong, R. Malaisamy, M.L. Bruening, Separation of fluoride from other monovalent anions using multilayer polyelectrolyte nanofiltration membranes, Langmuir 23 (2007) 1716–1722, https://doi.org/10.1021/la061701y.

[22] R. Epsztein, E. Shaulsky, M. Qin, M. Elimelech, Activation behavior for ion permeation in ion-exchange membranes: role of ion dehydration in selective transport, J. Membr. Sci. 580 (2019) 316–326, https://doi.org/10.1016/j.memsci.2019.02.009.

[23] S.T. Morthensen, J. Luo, A.S. Meyer, H. Jørgensen, M. Pinelo, High performance separation of xylose and glucose by enzyme assisted nanofiltration, J. Membr. Sci. 492 (2015) 107–115, https://doi.org/10.1016/j.memsci.2015.05.025.

[24] S. Faucher, N. Aluru, M.Z. Bazant, D. Blankschtein, A.H. Brozena, J. Cumings, J. Pedro De Souza, M. Elimelech, R. Epsztein, J.T. Fourkas, A.G. Rajan, H.J. Kulik, A. Levy, A. Majumdar, C. Martin, M. McEldrew, R.P. Misra, A. Noy, T.A. Pham, M. Reed, E. Schwegler, Z. Siwy, Y. Wang, M. Strano, Critical knowledge gaps in mass transport through single-digit nanopores: a review and perspective, J. Phys. Chem. C 123 (2019) 21309–21326, https://doi.org/10.1021/acs.jpcc.9b02178.

[25] L.A. Richards, B.S. Richards, B. Corry, A.I. Schäfer, Experimental energy barriers to anions transporting through nanofiltration membranes, Environ. Sci. Technol. 47 (2013) 1968–1976, https://doi.org/10.1021/es303925r.

[26] M. Zwolak, J. Wilson, M. Di Ventra, Dehydration and ionic conductance quantization in nanopores, J. Phys. Condens. Matter 22 (2010) 454126, https://doi.org/10.1088/0953-8984/22/45/454126.

[27] L.A. Richards, A.I. Schäfer, B.S. Richards, B. Corry, The importance of dehydration in determining ion transport in narrow pores, Small 8 (2012) 1701–1709, https://doi.org/10.1002/smll.201102056.

[28] B. Corry, Designing carbon nanotube membranes for efficient water desalination, J. Phys. Chem. B 112 (2008) 1427–1434, https://doi.org/10.1021/jp709845u.

[29] L.A. Richards, A.I. Schäfer, B.S. Richards, B. Corry, Quantifying barriers to monovalent anion transport in narrow non-polar pores, Phys. Chem. Chem. Phys. 14 (2012) 11633–11638, https://doi.org/10.1039/c2cp41641g.

[30] Y. Ruan, Y. Zhu, Y. Zhang, Q. Gao, X. Lu, L. Lu, Molecular dynamics study of Mg2+/Li+ separation via biomimetic graphene-based nanopores: the role of dehydration in second shell, Langmuir 32 (2016) 13778–13786, https://doi.org/10.1021/acs.langmuir.6b03001.

[31] K. Li, Y. Tao, Z. Li, J. Sha, Y. Chen, Selective ion-permeation through strained and charged graphene membranes, Nanotechnology 29 (2018), 035402, https://doi.org/10.1088/1361-6528/aa9b0c.

[32] S. Zhu, R.S. Kingsbury, D.F. Call, O. Coronell, Impact of solution composition on the resistance of ion exchange membranes, J. Membr. Sci. 554 (2018) 39–47, https://doi.org/10.1016/j.memsci.2018.02.050.

[33] O.N. Samoylova, E.I. Calixte, K.L. Shuford, Molecular dynamics simulations of ion transport in carbon nanotube channels, J. Phys. Chem. C 119 (2015) 1659–1666, https://doi.org/10.1021/jp5103669.

[34] L. Paugam, C.K. Diawara, J.P. Schlumpf, P. Jaouen, F. Quéméneur, Transfer of monovalent anions and nitrates especially through nanofiltration membranes in brackish water conditions, Separ. Purif. Technol. 40 (2004) 237–242, https://doi.org/10.1016/j.seppur.2004.02.012.

[35] L. Wang, M.S.H. Boutilier, P.R. Kidambi, D. Jang, N.G. Hadjiconstantinou, R. Karnik, Fundamental transport mechanisms, fabrication and potential applications of nanoporous atomically thin membranes, Nat. Nanotechnol. 12 (2017) 509–522, https://doi.org/10.1038/nnano.2017.72.

[36] K. Sint, B.Y. Wang, P. Kral, Selective ion passage through functionalized graphene nanopores, J. Am. Chem. Soc. 131 (2009) 16448–16449, https://doi.org/10.1021/ja903655u.

[37] R. Epsztein, E. Shaulsky, N. Dizge, D.M. Warsinger, M. Elimelech, Role of ionic charge density in donnan exclusion of monovalent anions by nanofiltration, Environ. Sci. Technol. 52 (2018) 4108–4116, https://doi.org/10.1021/acs.est.7b06400.

[38] B.J. Zwolinski, H. Eyring, C.E. Reese, Diffusion and membrane permeability, J. Phys. Colloid Chem. 53 (1949) 1426–1453, https://doi.org/10.1021/j150474a012.

[39] M. Ding, A. Szymczyk, A. Ghoufi, On the structure and rejection of ions by a polyamide membrane in pressure-driven molecular dynamics simulations, Desalination 368 (2015) 76–80, https://doi.org/10.1016/j.desal.2015.01.003.

[40] T. Arfin, Rafiuddin, Metal ion transport through a polystyrene-based cobalt arsenate membrane: application of irreversible thermodynamics and theory of absolute reaction rates, Desalination 284 (2012) 100–105, https://doi.org/10.1016/j.desal.2011.08.042.

[41] T.R. Farhat, J.B. Schlenoff, Doping-controlled ion diffusion in polyelectrolyte multilayers: mass transport in reluctant exchangers, J. Am. Chem. Soc. 125 (2003) 4627–4636, https://doi.org/10.1021/ja021448y.

[42] S. Na, T. Steinbrecher, T. Koslowski, Thermodynamic integration network approach to ion transport through protein channels: perspectives and limits, J. Comput. Chem. 39 (2018) 2539–2550, https://doi.org/10.1002/jcc.25615.

[43] T.R. Farhat, J.B. Schlenoff, Ion transport and equilibria in polyelectrolyte multilayers, Langmuir 17 (2001) 1184–1192, https://doi.org/10.1021/la001298+.

[44] H. Nada, T. Sakamoto, M. Henmi, T. Ogawa, M. Kimura, T. Kato, Environmental Science Ions in Sub-nano Channels of Nanostructured, 2019, https://doi.org/10.1039/c9ew00842j.

[45] D.G. Truhlar, B.C. Garrett, Variational transition state theory, Annu. Rev. Phys. Chem. 35 (1984) 159–189.

[46] J. Abraham, K.S. Vasu, C.D. Williams, K. Gopinadhan, Y. Su, C.T. Cherian, J. Dix, E. Prestat, S.J. Haigh, I.V. Grigorieva, P. Carbone, A.K. Geim, R.R. Nair, Tunable sieving of ions using graphene oxide membranes, Nat. Nanotechnol. 12 (2017) 546–550, https://doi.org/10.1038/nnano.2017.21.

[47] N. Dizge, R. Epsztein, W. Cheng, C.J. Porter, M. Elimelech, Biocatalytic and salt selective multilayer polyelectrolyte nanofiltration membrane, J. Membr. Sci. 549 (2018) 357–365, https://doi.org/10.1016/j.memsci.2017.12.026.

[48] S.U. Hong, R. Malaisamy, M.L. Bruening, Optimization of flux and selectivity in Cl-/SO42- separations with multilayer polyelectrolyte membranes, J. Membr. Sci. 283 (2006) 366–372, https://doi.org/10.1016/j.memsci.2006.07.007.

[49] X. Zan, B. Peng, D.A. Hoagland, Z. Su, Polyelectrolyte uptake by PEMs: impact of salt concentration, Polym. Chem. 2 (2011) 2581–2589, https://doi.org/10.1039/c1py00280e.

[50] E. Hübsch, V. Ball, B. Senger, G. Decher, J.C. Voegel, P. Schaaf, Controlling the growth regime of polyelectrolyte multilayer films: changing from exponential to linear growth by adjusting the composition of polyelectrolyte mixtures, Langmuir 20 (2004) 1980–1985, https://doi.org/10.1021/la0361870.

[51] M. Adusumilli, M.L. Bruening, Variation of ion-exchange capacity, ζ potential, and ion-transport selectivities with the number of layers in a multilayer polyelectrolyte film, Langmuir 25 (2009) 7478–7485, https://doi.org/10.1021/la900391q.

[52] T. Radeva, V. Milkova, I. Petkanchin, Electro-optics of colloids coated with multilayers from strong polyelectrolytes:surface charge relaxation, J. Colloid Interface Sci. 266 (2003) 141–147, https://doi.org/10.1016/S0021-9797(03)00533-2.

[53] D.M. Reurink, J.P. Haven, I. Achterhuis, S. Lindhoud (Erik), H.D.W. Roesink, W. M. de Vos, Annealing of polyelectrolyte multilayers for control over ion permeation, Adv. Mater. Interfaces. 5 (2018) 1800651, https://doi.org/10.1002/admi.201800651.

[54] J.A. Jaber, J.B. Schlenoff, Counterfoils and water in polyelectrolyte multilayers: a tale of two polycations, Langmuir 23 (2007) 896–901, https://doi.org/10.1021/la061839g.

[55] H.M. Fares, Y.E. Ghoussoub, R.L. Surmaitis, J.B. Schlenoff, Toward ion-free polyelectrolyte multilayers: cyclic salt annealing, Langmuir 31 (2015) 5787–5795, https://doi.org/10.1021/la504910y.

[56] W.M. Deen, Hindered transport of large molecules in liquid-filled pores, AIChE J. 33 (1987) 1409–1425.

[57] L.D. Nghiem, A.I. Schafer, M. Elimelech, Removal of natural hormones by nanofiltration Membranes : measurement, modeling, and mechanisms, Environ. Eng. 38 (2004) 1888–1896, https://doi.org/10.1021/es034952r.

[58] R.A. Ghostine, R.M. Jisr, A. Lehaf, J.B. Schlenoff, Roughness and salt annealing in a polyelectrolyte multilayer, Langmuir 29 (2013) 11742–11750, https://doi.org/10.1021/la401632x.

[59] W.R. Bowen, J.S. Welfoot, Modelling the performance of membrane nanofiltration-critical assessment and model development, Chem. Eng. Sci. 57 (2002) 1121–1137, https://doi.org/10.1016/S0009-2509(01)00413-4.

[60] B. Van der Bruggen, M. Mänttäri, M. Nyström, Drawbacks of applying nanofiltration and how to avoid them : a review, Separ. Purif. Technol. 63 (2008) 251–263, https://doi.org/10.1016/j.seppur.2008.05.010.

[61] V. Freger, T.C. Arnot, J.A. Howell, Separation of concentrated organic/inorganic salt mixtures by nanofiltration, J. Membr. Sci. 178 (2000) 185–193, https://doi.org/10.1016/S0376-7388(00)00516-0.

[62] H.H. Kim, J.H. Kim, Y.K. Chang, Removal of potassium chloride by nanofiltration from ion-exchanged solution containing potassium clavulanate, Bioproc. Biosyst. Eng. 33 (2010) 149–158, https://doi.org/10.1007/s00449-009-0360-7.

[63] R.R. Sharma, S. Chellam, Temperature and concentration effects on electrolyte transport across porous thin-film composite nanofiltration membranes: pore transport mechanisms and energetics of permeation, J. Colloid Interface Sci. 298 (2006) 327–340, https://doi.org/10.1016/j.jcis.2005.12.033.

[64] R.W. Tsien, D. Noble, A transition state theory approach to the kinetics of conductance changes in excitable membranes, J. Membr. Biol. 1 (1969) 248–273, https://doi.org/10.1007/BF01869785.